A SPATIAL AND SPECTRAL STUDY OF NONTHERMAL FILAMENTS IN HISTORICAL SUPERNOVA REMNANTS: OBSERVATIONAL RESULTS WITH *CHANDRA*

AYA BAMBA,[1] RYO YAMAZAKI,[2] TATSUO YOSHIDA,[3] TOSHIO TERASAWA,[4] AND KATSUJI KOYAMA[5]
Received 2004 June 30; accepted 2004 November 10

ABSTRACT

The outer shells of young supernova remnants (SNRs) are the most plausible acceleration sites of high-energy electrons with the diffusive shock acceleration (DSA) mechanism. We studied spatial and spectral properties close to the shock fronts in four historical SNRs (Cas A, Kepler's remnant, Tycho's remnant, and RCW 86) with excellent spatial resolution of *Chandra*. In all of the SNRs, hard X-ray emissions were found on the rims of the SNRs, which concentrate in very narrow regions (so-called filaments); apparent scale widths on the upstream side are below or on the order of the point-spread function of *Chandra*, while they are $0\rlap{.}{''}5$–$40''$ (0.01–0.4 pc) on the downstream side with most reliable distances. The spectra of these filaments can be fitted with both thermal and nonthermal (power law and SRCUT) models. The former requires unrealistic high temperature ($\gtrsim 2$ keV) and low abundances ($\lesssim 1$ solar) for emission from young SNRs and may be thus unlikely. The latter reproduces the spectra with best-fit photon indices of 2.1–3.8, or roll-off frequencies of $(0.1-28) \times 10^{17}$ Hz, which reminds us of the synchrotron emission from electrons accelerated via DSA. We consider various physical parameters as functions of the SNR age, including the previous results on SN 1006; the filament width on the downstream side increases with the SNR age, and the spectrum becomes softer, keeping a nonthermal feature. It was also found that a function, that is, the roll-off frequency divided by the square of the scale width on the downstream side, shows negative correlation with the age, which might provide us some information on the DSA theory.

Subject headings: acceleration of particles — ISM: individual (Cassiopeia A, Kepler's Supernova Remnant, G120.1+1.4, SN 1006, RCW 86) — supernova remnants — X-rays: ISM

1. INTRODUCTION

Ever since the discovery of cosmic rays (Hess 1912), the origin and the acceleration mechanism up to more than ∼TeV have been long-standing problems. Koyama et al. (1995) discovered synchrotron X-rays from shock fronts of a supernova remnant (SNR), SN 1006, and suggested that shocks of SNRs are cosmic-ray accelerators. Several SNRs have recently been categorized into synchrotron X-ray emitters (G347.3−0.5, Koyama et al. 1997; Slane et al. 1999; RCW 86, Bamba et al. 2000; Borkowski et al. 2001b; G266.6−1.2, Slane et al. 2001). Recently, a significant number of SNRs with synchrotron X-rays have been discovered by the *ASCA* Galactic plane survey (Bamba et al. 2001, 2003a; Ueno et al. 2003; Yamaguchi et al. 2005). These discoveries provide good evidence for the cosmic-ray acceleration at the shocked shell of SNRs. The most plausible process of the cosmic-ray acceleration is the diffusive shock acceleration (DSA; e.g., Bell 1978; Blandford & Ostriker 1978; Drury 1983; Blandford & Eichler 1987; Jones & Ellison 1991; Malkov & Drury 2001), which can accelerate particles on the shock into a power-law distribution, similar to the observed spectrum of cosmic rays showering on the Earth.

Apart from the global success of DSA, there are still many remaining problems. We have not yet fully understood detailed but important information, such as the maximum energy of particles, the configuration of magnetic fields, the injection efficiency from thermal plasma to accelerated particles, the acceleration and de-acceleration history of particles around the shock fronts, and so on. This partly comes from the fact that there is no information about the spatial distribution of accelerated electrons of practical objects, which strongly reflects the above uncertainties.

Bamba et al. (2003b) considered the spatial distribution of emission from accelerated particles as new information in order to understand the acceleration on the shock in SNRs; they observed the synchrotron X-ray–emitting shell of SN 1006 with the excellent spatial resolution of *Chandra* (see also Long et al. 2003) and found that the emitting regions of synchrotron X-rays are incredibly thin ("filaments"), about 0.01–0.1 pc on the upstream side and 0.06–0.4 pc on the downstream side, at 2.18 kpc distance (Winkler et al. 2003). This result constrains the DSA theory and magnetic field configurations; both an efficient acceleration scenario with strong magnetic field parallel to the shock normal and an inefficient one with a weak and perpendicular magnetic field are allowed (Yamazaki et al. 2004; Berezhko et al. 2003).

In the present work we searched for nonthermal filaments in other historical SNRs (Cas A, Kepler's remnant, Tycho's remnant, and RCW 86) and measured their scale widths and spectral parameters. It was also investigated whether or not the age of the SNR is correlated with the scale width and/or spectral parameters of filaments. If it is, such correlations might describe the time evolution of these parameters in a single SNR. Although the characteristics of the SNR should be considered, those correlations may also become clues to understand the time evolution

[1] RIKEN (The Institute of Physical and Chemical Research) 2-1, Hirosawa, Wako, Saitama 351-0198, Japan; bamba@crab.riken.jp.

[2] Department of Earth and Space Science, Graduate School of Science, Osaka University, Toyonaka, Osaka 560-0043, Japan; ryo@vega.ess.sci.osaka-u.ac.jp.

[3] Faculty of Science, Ibaraki University, Mito 310-8512, Japan; yoshidat@mx.ibaraki.ac.jp.

[4] Earth and Planetary Science, Graduate School of Science, University of Tokyo, 7-3-1, Hongo, Bunkyo-ku, Tokyo 113-0033, Japan; terasawa@eps.s.u-tokyo.ac.jp.

[5] Department of Physics, Graduate School of Science, Kyoto University, Sakyo-ku, Kyoto 606-8502, Japan; koyama@cr.scphys.kyoto-u.ac.jp.

TABLE 1

Observation Log

Target	Type	ObsID	R.A.	Decl.	Date	Exposure (ks)
Cas A	Ib	00114	23 23 40.2	58 47 34.1	2000 Jan 30–31	50
Kepler...................................	?	00116	17 30 39.6	−21 30 32.5	2000 Jun 30–Jul 1	49
Tycho....................................	Ia	00115	10 25 07.0	64 09 44.7	2000 Sep 20–21	49
SN 1006	Ia	00732	15 03 51.6	−41 51 18.8	2000 Jul 10–11	68
Southwestern shell of RCW 86..........	II?	01993	14 40 46.6	−62 39 43.9	2001 Feb 1–2	92

Note.—Units of right ascension are hours, minutes, and seconds, and units of declination are degrees, arcminutes, and arcseconds.

of the maximum energy of electrons, the magnetic field configuration, the injection efficiency, and so on. This paper is organized as follows. We summarize the observation details of five SNRs with *Chandra* in § 2. In § 3 we briefly describe the results of the observations of the four SNRs. In § 4 we discuss the origin of emission (§ 4.1), our analysis of individual SNRs (§ 4.2), and the time evolution of the spatial and spectral parameters of filaments together with previous analysis of SN 1006, which have already been analyzed in Bamba et al. (2003b) (§ 4.3). We also briefly deal with the time evolution of energy densities of the magnetic field and cosmic rays in this section. A summary of our results is given in § 5.

2. OBSERVATIONS

We used the *Chandra* archival data of the ACIS of five historical SNRs (Cas A, Kepler, Tycho, SN 1006, and RCW 86), as listed in Table 1. Note that this data set includes almost historical shell-type SNRs. The satellite and the instrument are described by Weisskopf et al. (2002) and Garmire et al. (2000), respectively. Data acquisition from the ACIS was made in the Timed-Exposure Faint mode. The data reductions and analysis were made using the *Chandra* Interactive Analysis of Observations (CIAO) software version 2.3. Using the level 2 processed events provided by the pipeline processing at the *Chandra* X-Ray Center, we selected *ASCA* grades 0, 2, 3, 4, and 6 as the X-ray events. The effective exposure for each observation is also given in Table 1.

3. INDIVIDUAL RESULTS

3.1. *Cas A (G111.7−2.1)*

Although the remnant's precise age is still uncertain, the most probable record of the explosion is SN 1680, made by Flamsteed (1725), which we adopt in this paper. The distance to the remnant was estimated to be $3.4^{+0.3}_{-0.1}$ kpc by Reed et al. (1995) using the measurement of optical proper motions. The average radio index of the whole remnant at 1 GHz is 0.78 (Green 2004).

Cas A emits hard X-rays up to greater than 10 keV, which were detected by *RXTE* (Allen et al. 1997), *BeppoSAX* (Favata et al. 1997), and OSSE on board the *Compton Gamma Ray Observatory* (*CGRO*; The et al. 1996). Vink & Laming (2003) have already found and analyzed one of the nonthermal filamentary structures with *Chandra*. There are many other filaments thinner than that which they analyzed. These filaments are considered to be profiles of a thin sheetlike structure, as suggested by Hester (1987); then, the scale width of these filaments is the upper limit width of the real thickness in the radial direction of the sheets. Therefore, we consider other filaments in this paper, which are located much nearer to the aim point (less than 25″) and are much thinner than those analyzed by Vink & Laming (2003).

The top left panel of Figure 1 shows the southeastern side of Cas A in the 5.0–10.0 keV band, in which there are a lot of filamentary structures. These filaments are more clumpy than those in SN 1006 (Bamba et al. 2003b). We selected two filaments as shown in the panel, which are straight enough to be made profiles and near the aim point.

Figures 2a and 2b show the profiles of two filaments. In order to estimate the scale width of these filaments, we used a simple, empirical fitting model for the apparent profiles, which is the same as used in the previous analysis in the SN 1006 case by Bamba et al. (2003b):

$$f(x) = \begin{cases} A \exp\left(-\left|\dfrac{x_0 - x}{w_u}\right|\right), & \text{upstream side,} \\[2ex] A \exp\left(-\left|\dfrac{x_0 - x}{w_d}\right|\right), & \text{downstream side,} \end{cases} \quad (1)$$

where A and x_0 are the flux and position at the emission peak, respectively. The quantities w_u and w_d represent the *e*-folding widths on the upstream and the downstream sides of the apparent emission peak, respectively (hereafter "*u*" and "*d*" represent upstream and downstream sides, respectively). We treat the best-fit values smaller than 0″8 as the upper limit because they highly suffer the influence of the point-spread function (PSF), which is about 0″5 within ~4′ radius from the aim point. The fittings were made with profiles in the 5.0–10.0 keV band and were accepted statistically with the best-fit models and parameters shown in Figures 2a and 2b and Table 2.

We then made the spectra of the filaments within the scale widths ($x_0 - w_u \leq x \leq x_0 + w_d$) in Figures 2a and 2b. The background spectra were made from the just off-filament downstream sides with the same width of the filaments. We compared the Si line photon counts with those in the continuum (5.0–10.0 keV) band in these regions and found that photons in this band include thermal photons in a ratio of only less than 25%, under the assumption that all photons in the background regions are thermal, and both regions have a thermal component with the same physical parameters, except for their flux. Therefore, we treated all the 5.0–10.0 keV photons in our analysis of Cas A, as part of the hard X-rays reported in previous observations (Vink & Laming 2003).

The background-subtracted spectrum accumulated from the two filaments is shown in the top left panel of Figure 3, which is featureless with no linelike structure and extends to the hard X-ray side, which was fitted with both an absorbed thin thermal plasma model in nonequilibrium ionization (NEI) calculated by Borkowski et al. (2001a; NEI model) and an absorbed power-law model. The absorption column was subsequently calculated using the cross sections by Morrison & McCammon (1983) with the solar abundances (Anders & Grevesse 1989). Both models
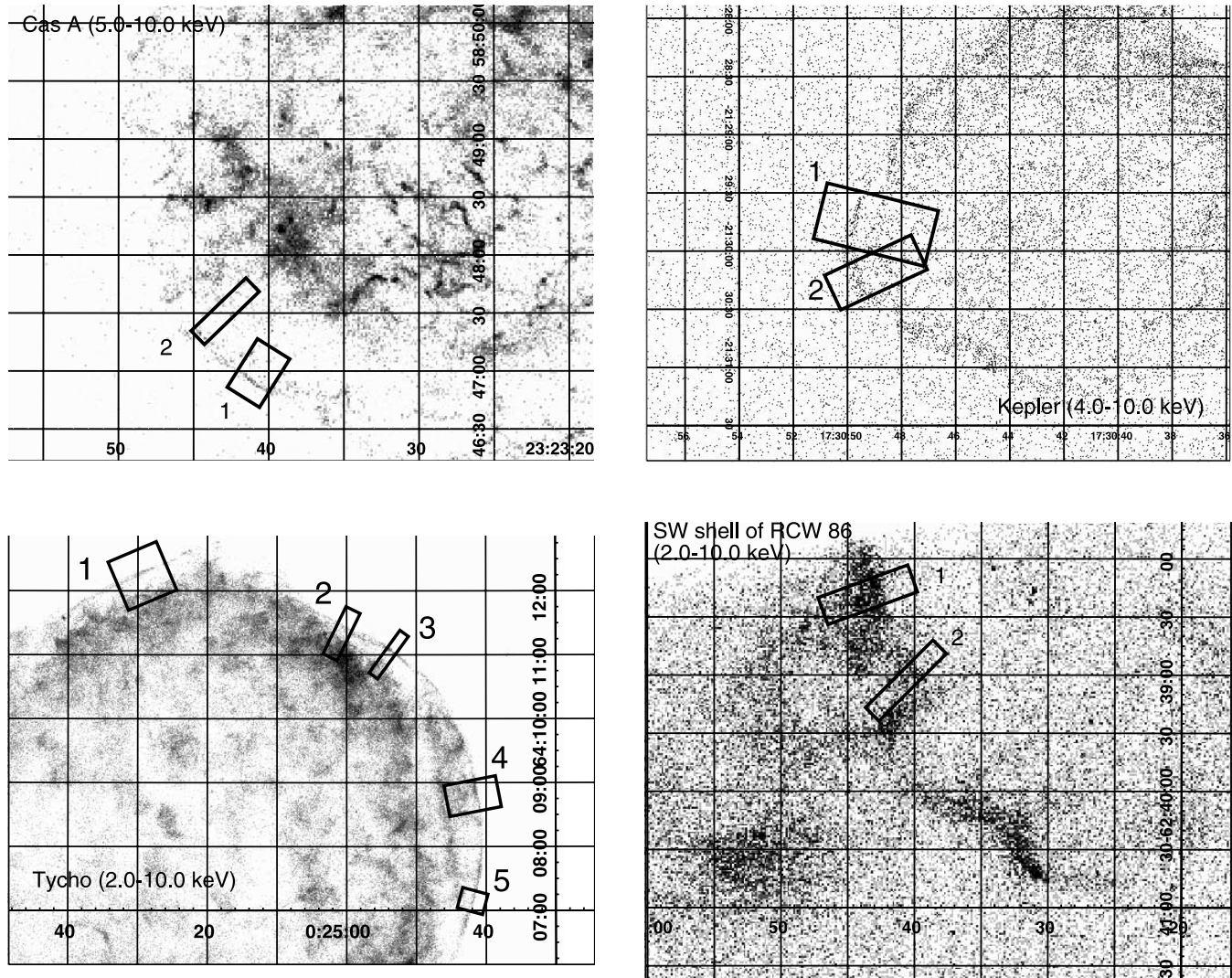
Fig. 1.—Close-up views of the SNRs in the hard X-ray band (written in each image; also see text) with *Chandra*. Gray scales are in logarithmic and coordinates are in J2000.0. The filament regions for spatial and spectral analyses are also shown by solid rectangles.

were well fitted statistically with best-fit curves and parameters, shown in Figure 3 and Table 3. We also applied the SRCUT model, which represents the synchrotron emission from electrons of power-law distribution with exponential roll-off in a homogeneous magnetic field (Reynolds 1998; Reynolds & Keohane 1999). The spectral index at 1 GHz was fixed to be 0.78 according to a report by Green (2004). This model also well reproduces the spectra with best-fit values shown in Table 3. The spectra are much harder than those of the filament analyzed by Vink & Laming (2003).

3.2. *Kepler's Remnant (G4.5+6.8)*

Kepler's remnant, which appeared in 1604 (Kepler 1606), is the second youngest SNR in our Galaxy recorded by human beings. DeLaney et al. (2002) observed this SNR with VLA[6] and found a spatial variation of the spectral index from 0.85 to 0.6, with a mean value of 0.7. The distance to the remnant is 4.8 ± 1.4 kpc using the H I observations with VLA (Reynoso & Goss 1999). Petre et al. (1999) found hard X-rays (above 10 keV)

from Kepler with *RXTE*, and *XMM-Newton* pointed out that at least the southeastern edge emits nonthermal X-rays (Cassam-Chenaï et al. 2004).

The top right panel of Figure 1 shows a 4.0–10.0 keV band *Chandra* image of the eastern rim of Kepler. We can see very sharp structures on the outer edge of the remnant, especially bright on the eastern side, which is similar to the filaments in SN 1006. In order to carry out spatial and spectral analysis of these structures, we selected two filaments, as shown in the panel, which are $<160''$ distant from the aim point. Figures 2c and 2d show the profiles of the filaments in the 4.0–10.0 keV band. They have sharp edges on both the upstream and downstream sides of the emission peak, and equation (1) well represents their profiles with best-fit curves and parameters summarized in the panels and Table 2.

We obtained the spectra of these filaments in the same way as in the Cas A case. Background regions were selected just from the downstream sides of the filaments, which are free from any other structures. The intensities of iron and silicon lines and continuum photons in the 4.0–10.0 keV band were compared, and it was found that more than 90% of the photons in the 4.0–10.0 keV band are the hard X-ray component reported in previous observations (Petre et al. 1999; Cassam-Chenaï et al.

---

[6] The National Radio Astronomy Observatory is a facility of the National Science Foundation operated under cooperative agreement by Associated Universities, Inc.
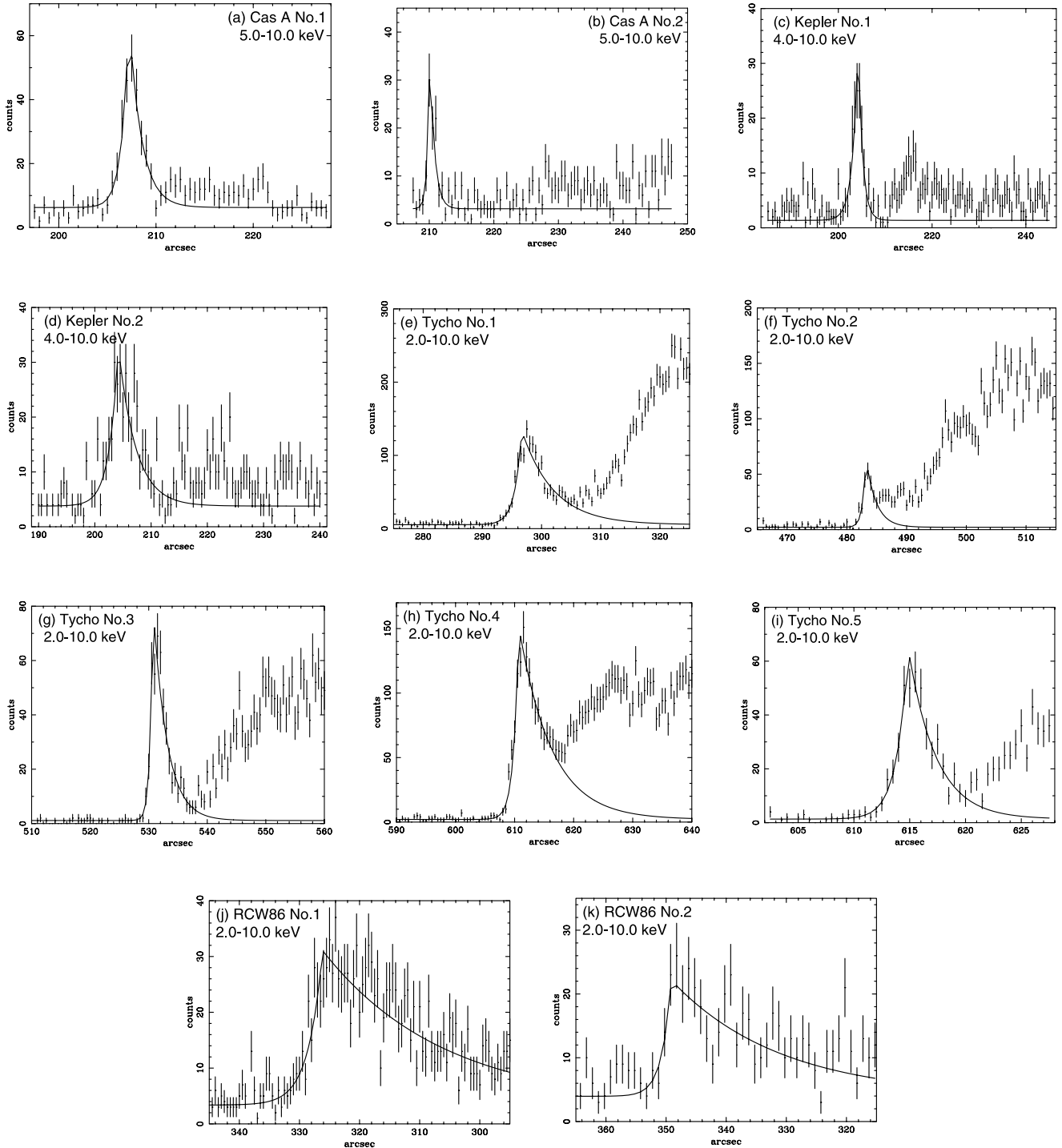
FIG. 2.—Profiles of the filaments of SNRs in the hard X-ray band (Cas A: 5.0–10.0 keV; Kepler: 4.0–10.0 keV; Tycho: 2.0–10.0 keV; RCW 86: 2.0–10.0 keV). The best-fit models are shown by solid lines. The shock runs from right to left in all the panels. Note that fittings were carried out in a part around the shock front in order to avoid any contamination from bright thermal emission.

2004), with the same assumptions as in the Cas A case. Thus, the derived scale widths represent those of the hard X-ray emission. The background-subtracted spectrum accumulated from these filaments is shown in the top right panel of Figure 3, which shows a hard and lineless feature. We fitted each spectrum with NEI and power-law models with an absorption. Both models are well fitted to the data, with the best-fit models and parameters shown in the panel and Table 3. The SRCUT model was also applied with the spectral index at 1 GHz fixed to be 0.70, derived by DeLaney et al. (2002) as the average value on

the eastern side. This model also well represents the data with the best-fit parameters listed in Table 3.

3.3. Tycho's Remnant (G120.1+1.4)

Tycho is a remnant of a supernova that exploded in 1572 (Tycho 1573). The distance to the remnant is estimated to be 1.5–3.1 kpc, from the proper motion of the optical filaments (Kamper & van den Bergh 1978) and the shock velocity estimated by Ghavamian et al. (2001). We adopt the most popular value, 2.3 kpc. Katz-Stone et al. (2000) investigated the

Number	A (counts arcsec^{-1})	w_u (arcsec)	w_d (arcsec)	Reduced χ^2 (χ^2/dof)
Cas A				
1......................................	59 (46–72)	(<0.93)	1.27 (0.96–1.81)	99.7/61
2......................................	34 (24–49)	(<0.80)	(<1.59)	27.3/26
Kepler				
1......................................	33 (26–41)	1.17 (0.87–1.59)	0.93 (<1.41)	19.3/21
2......................................	29 (25–34)	1.59 (1.17–2.19)	3.09 (3.46–3.87)	70.1/47
Tycho				
1......................................	129 (119–139)	1.18 (1.01–1.32)	5.36 (4.47–6.12)	82.7/55
2......................................	62 (48–70)	(<0.80)	1.70 (1.32–3.15)	42.3/32
3......................................	80 (74–83)	(<0.80)	2.38 (2.20–2.54)	23.4/37
4......................................	150 (146–152)	0.86 (0.80–0.93)	5.53 (5.00–6.14)	48.9/46
5......................................	63 (57–71)	1.03 (0.90–1.35)	2.47 (1.93–3.15)	17.9/21
RCW 86				
1......................................	28 (25–30)	2.39 (1.48–3.34)	20.1 (17.3–23.8)	113.4/95
2......................................	18 (14–23)	1.56 (0.49–4.79)	18.2 (11.8–35.6)	46.8/31

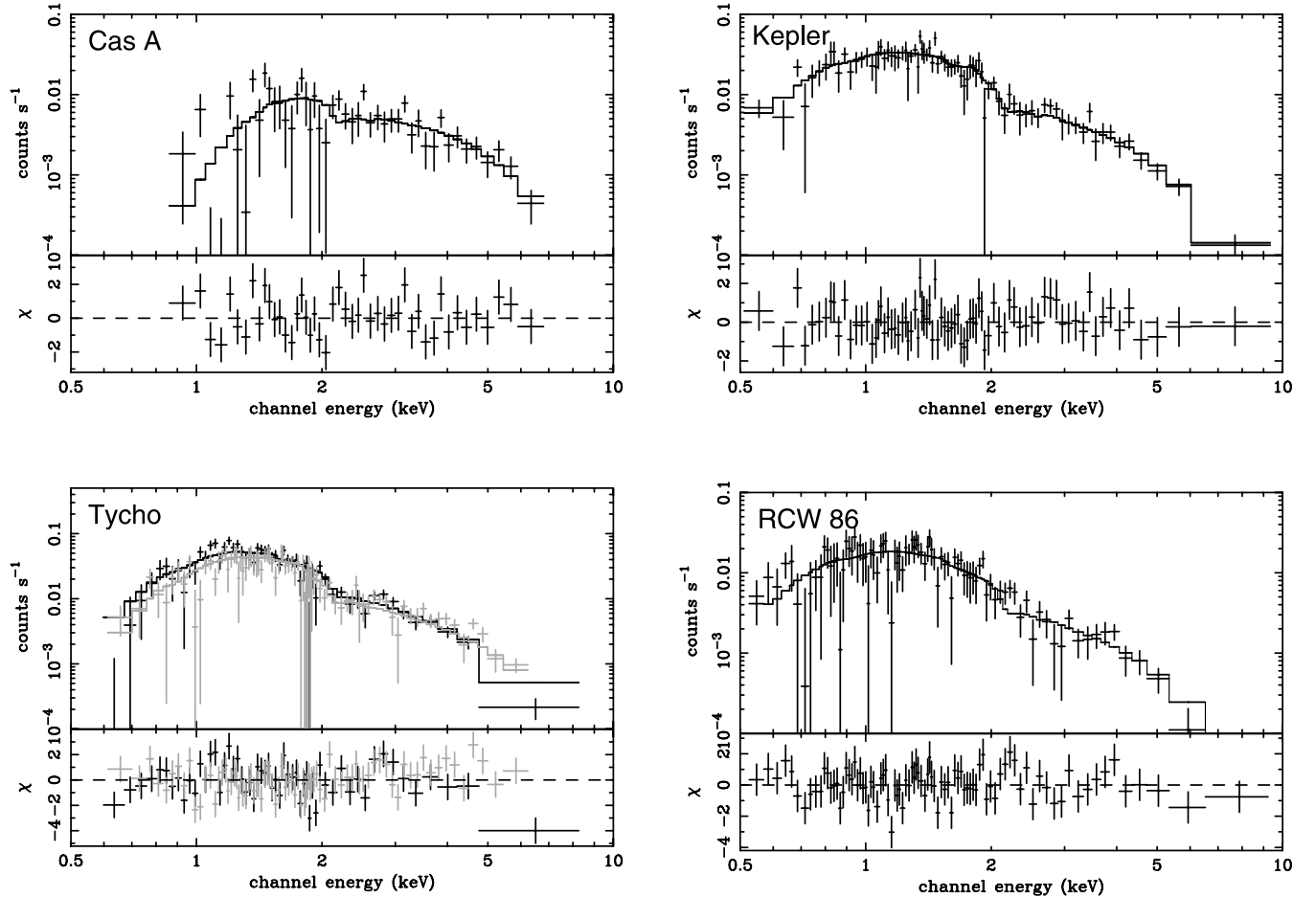NOTE.—Parentheses indicate single-parameter 90% confidence regions.

FIG. 3.—Spectra of combined filaments for each SNR (*crosses*). The best-fit power-law models are shown by the solid lines. The black and gray crosses in the panel for Tycho are the spectra accumulated from filaments on the different CCD chips. The lower section of each panel represents the residuals from the best-fit model.

TABLE 3
BEST-FIT PARAMETERS OF SPECTRAL FITTINGS OF FILAMENTS

			NEI			
NUMBER	kT (keV)	Z[b]	$n_e t$[c] (10^{10} s cm^{-3})	EM[d] (10^{55} cm^{-3})	N_H[e] (10^{21} cm^{-2})	χ^2/dof

Cas A

1................	5.4 (>2.1)	0.28 (<1.4)	[i]	3.6 (2.0–8.1)	27 (15–41)	28.0/31
2................	5.7 (2.7–34)	(>0.19)	0.030 (0.011–0.096)	0.15 (0.073–3.5)	17 (11–25)	19.1/27
Total	5.4 (3.0–13)	0.26 (0.019–0.73)	3.8 (1.6–7.7)	5.6 (4.1–9.3)	25 (17–35)	56.4/42

Kepler

1................	3.5 (2.7–4.9)	(<0.067)	8.2 (3.4–28)	5.5 (4.5–6.8)	4.3 (3.4–5.6)	43.2/52
2................	3.0 (2.5–3.8)	0.13 (<0.40)	[i]	7.9 (6.5–9.7)	3.7 (3.0–4.5)	25.7/30
Total	3.2 (2.6–3.9)	(<0.34)	11 (>6.9)	14 (12–17)	4.0 (3.4–4.7)	47.6/53

Tycho

1................	1.9 (1.6–2.4)	0.22 (0.062–0.50)	3.4×10^3 (>69)	4.7 (3.5–6.0)	6.5 (5.4–7.5)	102.3/68
2................	1.0 (0.58–6.9)	(<1.6)	[i]	2.5 (0.27–9.2)	12 (6.6–20)	9.40/11
3................	2.1 (1.6–2.9)	0.12 (<0.37)	[i]	1.7 (0.85–2.4)	11 (5.7–15)	40.2/41
4................	4.3 (3.0–7.0)	(<0.38)	[i]	2.9 (2.3–3.9)	5.1 (3.4–10)	39.5/32
5................	1.8 (1.4–2.6)	0.05 (<0.20)	[i]	2.0 (1.1–3.2)	9.8 (5.1–14)	51.9/47
Total	2.3 (2.0–2.6)	0.07 (<0.17)	[i]	12 (11–14)	5.8 (5.2–6.4)	182.0/134

RCW 86

1................	2.5 (1.8–3.4)	0.032 (<0.12)	[i]	2.1 (1.6–2.8)	5.7 (3.3–8.3)	67.2/58
2................	1.4 (1.0–2.2)	0.27 (0.019–1.0)	0.35 (0.20–0.52)	0.82 (0.49–1.4)	7.0 (3.2–9.4)	18.7/25
Total	2.1 (1.6–2.6)	0.11 (<0.25)	0.43 (<0.80)	3.3 (2.1–4.3)	7.0 (3.1–9.1)	75.3/85

		POWER-LAW				SRCUT[a]		
NUMBER	Γ	N_H[e] (10^{21} cm^{-2})	Flux[f] (10^{-13} ergs cm^{-2} s^{-1})	χ^2/dof	$\nu_{\text{roll-off}}$[g] (10^{17} Hz)	N_H[e] (10^{21} cm^{-2})	$\Sigma_{1\,\text{GHz}}$[h] (0.1 Jy)	χ^2/dof

Cas A

1................	2.3 (2.0–3.5)	27 (20–47)	1.9	29.2/33	9.3 (>4.5)	26 (20–33)	6.3 (5.1–7.6)	29.2/33
2................	2.2 (1.9–2.8)	20 (13–31)	1.1	22.1/29	28 (>1.3)	20 (16–24)	2.1 (1.7–2.4)	22.1/29
Total	2.1 (1.6–2.7)	23 (15–34)	3.1	57.6/44	24 (>1.8)	22 (19–27)	6.3 (5.4–7.2)	57.6/44

Kepler

1................	2.3 (2.1–2.5)	5.8 (4.8–7.0)	1.7	42.2/54	5.5 (2.1–17)	5.3 (4.7–6.0)	0.90 (0.83–0.98)	42.8/54
2................	2.4 (2.2–2.6)	5.5 (4.5–6.7)	2.2	24.9/32	4.0 (1.8–9.8)	4.9 (4.3–5.5)	1.4 (1.3–1.5)	25.0/32
Total	2.4 (2.2–2.6)	5.7 (4.9–6.6)	4.1	44.9/55	3.6 (2.0–7.9)	5.2 (4.8–5.7)	2.8 (2.6–3.0)	45.5/55

Tycho

1................	3.0 (2.8–3.3)	9.1 (7.9–11)	3.4	104.8/70	0.40 (0.25–0.70)	8.1 (7.4–8.8)	0.70 (0.64–0.77)	106.0/70
2................	3.8 (2.5–5.6)	16 (8.6–27)	0.49	9.05/13	0.11 (0.020–1.3)	14 (11–19)	1.4 (1.0–2.0)	9.15/13
3................	2.5 (2.2–2.9)	7.6 (6.0–9.8)	1.1	43.5/43	1.3 (0.52–4.5)	6.9 (5.9–8.2)	0.051 (0.045–0.059)	43.2/43
4................	2.1 (2.0–2.4)	6.8 (4.6–9.6)	4.4	40.9/34	6.5 (1.8–46)	6.2 (5.0–7.7)	0.052 (0.046–0.059)	40.6/34
5................	2.9 (2.5–3.3)	9.4 (6.9–13)	1.1	55.5/49	0.64 (0.26–1.7)	8.2 (6.7–10)	0.12 (0.10–0.14)	54.4/49
Total	2.7 (2.6–2.9)	8.0 (7.3–9.0)	11	187.7/136	0.83 (0.59–1.2)	7.2 (6.7–7.7)	0.78 (0.73–0.83)	185.2/136

RCW 86

1................	2.5 (2.2–2.8)	5.4 (4.3–6.9)	1.4	68.9/60	2.0 (0.77–5.9)	4.8 (4.2–5.7)	0.19 (0.17–0.22)	68.8/60
2................	2.5 (2.1–3.2)	2.7 (1.1–4.1)	0.32	25.7/27	1.3 (0.29–12)	2.3 (1.5–3.5)	0.051 (0.039–0.064)	25.0/27
Total	2.4 (2.2–2.7)	4.7 (4.2–6.0)	1.8	82.2/87	2.1 (1.0–5.9)	4.3 (3.7–5.0)	0.22 (0.20–0.25)	80.8/87

NOTE.—Parentheses indicate single-parameter 90% confidence regions.
[a] Photon index at 1 GHz is assumed according to the previous radio observations (see text).
[b] Abundance ratio relative to the solar value (Anders & Grevesse 1989).
[c] Ionization timescale, where n_e and t are the electron density and age of the plasma, respectively.
[d] Emission measure, with the assumed distance to SNRs according to the previous observations (see text).
[e] Absorption column, calculated using the cross sections by Morrison & McCammon (1983) with the solar abundances (Anders & Grevesse 1989).
[f] Observed flux in the 0.5–10.0 keV band.
[g] Roll-off frequency.
[h] Flux density at 1 GHz.
[i] Not determined.

variations of the radio spectral indices and found that the emission in the outer rim shows a trend that brighter clumps have a flatter spectral index than the average index of $s = 0.52 \pm 0.02$, perhaps as a result of either SNR blast waves and ambient medium interactions or internal inhomogeneities of the magnetic field within the remnant.

Hard X-ray emission has been unmistakably detected from Tycho, up to 30 keV, with *HEAO 1* (Pravdo & Smith 1979), *Ginga* (Fink et al. 1994), and *RXTE* (Petre et al. 1999). *Chandra* and *XMM-Newton* also observed Tycho's remnant, and the good spatial resolutions of instruments on board these satellites show the spatial variety of X-ray emission (Hwang et al. 2002; Decourchelle et al. 2001). Hwang et al. (2002) claimed that there is a thin structure encircling the SNR, the spectrum of which has lines with low equivalent widths.

In order to be clear as to whether the thin structure is a hard X-ray emitter or not, spatial and spectral analyses were conducted in the same way as in the cases for Cas A and Kepler. The bottom left panel of Figure 1 shows the northwestern part of the remnant in the 2.0–10.0 keV band. The thin filament-like structure suggested by Hwang et al. (2002) can be seen. Figures 2e–2i show profiles of the filaments selected in the panel, which are located within 120″ from the aim point. Very sharp rises and decays can be seen in all of the filaments. The fittings with equation (1) were performed only around the outermost peak of hard X-ray emission because thermal photons dominate in the downstream regions (*right side of each panel*), and they were accepted statistically with the best-fit models and parameters shown in these panels and Table 2.

Their spectra were obtained in the same way as in the Cas A case. Background spectra were accumulated from just the downstream side of the filaments. The bottom left panel of Figure 3 shows the background-subtracted spectra, which were combined with those of filaments in each CCD chip. Since both are hard and have no linelike structure, we fitted them with NEI, power-law, and SRCUT models with an absorption. We fixed the spectral index at 1 GHz to be 0.52, following Katz-Stone et al. (2000). All three models were accepted statistically with similar probability, with the best-fit values listed in Table 3. We compared the Si and S lines and the 2.0–10.0 keV continuum band intensity in the source spectrum with those in the background region, and it was found that only less than 6% of the thermal photons contribute in the 2.0–10.0 keV band. Therefore, it is likely that all the photons in the 2.0–10.0 keV band can be treated as pure nonthermal.

3.4. *RCW 86 (G315.4−2.3)*

RCW 86 was identified as being the oldest historical SNR by Clark & Stephenson (1977). They suggested that a progenitor of the remnant was reported in AD 185 in Later Han dynasty records (Fan You 432), although Chin & Huang (1994) claimed some doubt about the record. The spectral index at 1 GHz and the distance were measured to be 0.6 (Caswell et al. 1975) and 2.8 kpc (Rosado et al. 1996), respectively.

Strong hard X-rays have been detected from the remnant by *Ginga* (Kaastra et al. 1992) and *RXTE* (Petre et al. 1999). Using *ASCA* data, Bamba et al. (2000) and Borkowski et al. (2001b) independently found that the hard X-rays show a nonthermal feature and concentrate on the southwestern shell of the SNR. The *Chandra* observation with excellent spatial resolution reveals that the regions emitting nonthermal X-rays are very clumpy and different from those emitting thermal X-rays (Rho et al. 2002).

The bottom right panel of Figure 1 represents a close-up view of the southwestern shell in the 2.0–10.0 keV band. Clumpy structures can be seen, which have been already indicated as

nonthermal filaments by Rho et al. (2002). We selected two filaments for our analysis, which are bright in the hard-band image and are located <120″ from the aim point. Their profiles from the region indicated in the panel were made, as shown in Figures 2j and 2k. They show a sharp rise and a rather slow decay in the upstream and downstream sides of the emission peak, respectively. The fitting with equation (1) was carried out in the 2.0–10.0 keV band and was accepted statistically with best-fit models and the values shown in the panels and Table 2.

The spectra were made in the same way as in the former cases. The background regions were selected from the downstream side of the filaments without other structures. The emission is free from thermal photons, according to previous studies, especially in such a hard band (Rho et al. 2002). The bottom right panel of Figure 3 shows the background-subtracted spectrum, which was accumulated from both filaments. The spectral fittings were made with the three models (NEI, power-law, and SRCUT) with an absorption. We adopted the spectral index at 1 GHz with the value 0.6 derived by Caswell et al. (1975). All of the models well reproduced the data with the best-fit profiles and values given in the panels and Table 3.

4. DISCUSSION

4.1. *Emission Origin of Filaments*

Table 3 summarizes the spectral fittings for the filaments in the four SNRs to thermal (NEI) and nonthermal (power-law and SRCUT) models. Because all models give a similar reduced χ^2, we cannot distinguish which model is the best statistically to reproduce the spectra of the filaments. The thermal model fittings for all cases, however, require an unusually high temperature and a low abundance for young (ejecta dominated) SNRs. On the other hand, the best-fit photon indices in the power-law model are $\sim$2–3, which are similar to hard X-rays in other SNRs (e.g., Koyama et al. 1995). It reminds us of the synchrotron emission from electrons with a power-law distribution of index of $\Gamma = 1.5$ or softer, suggesting that these filaments are acceleration sites of electrons via the DSA mechanism. The fitting of the SRCUT model requires a roll-off frequency of about 1 keV, as shown in Table 3. In order to check the influence of uncertainty of the radio index s, we fitted the spectra with the frozen s of 0.5 and 0.9. For the $s = 0.5$ cases, which is the theoretical minimum indicated by the DSA, $\nu_{\text{roll-off}}$ remains unchanged within a factor of 2. On the other hand, the fittings with $s = 0.9$, which implies that the de-acceleration is very efficient, require the change of $\nu_{\text{roll-off}}$ on the order of 1. However, the best-fit normalization in the radio band becomes larger than 10% of the total flux from the whole SNR, which is unrealistic for such small regions. Moreover, in the Kepler case, the radio map shows that the value of s of the rim is smaller than that of the inner region (DeLaney et al. 2002), although it changes from 0.85 to 0.6. This result suggests that the outer rims of SNRs are acceleration sites and de-acceleration may not occur yet, in other words, s is around 0.6. For the Tycho case, Katz-Stone et al. (2000) indicated that the spectral index of filaments in the outer rim is around 0.5, indicating that $\nu_{\text{roll-off}}$ derived in our analysis for the SNR is roughly correct. These results indicate that the X-ray photons shown in Figure 1 are emitted by electrons with the highest energy in each SNR.

It can be argued that the thermal spectra in source and background regions may be the same. The line emission from the NEI plasma changes as the ionization timescale ($n_e t$) varies. We take the background regions just behind the source regions, and their widths are much smaller (1%–5% of SNR radii). The

electron density n_e may not change so drastically in such thin downstream regions. Thus, the difference of $n_e t$ between the background and source regions may not be large enough to clarify the difference between their thermal spectra.

All of the filaments have much smaller scale widths than that derived from the Sedov self-similar solution ($=R/12$), on both the upstream and downstream sides, which is similar to the previous results in the SN 1006 case (Bamba et al. 2003b). We should consider the influence of PSF, especially for the filaments in Cas A and Tycho, where w_u are as small as the PSF (see Table 2). The PSF enlarges the apparent w_u and w_d. Thus, our result may be the upper limit of the physical scale width. Together with the fact that our sample covers almost historical SNRs with an X-ray shell, it may be suggested that all relative young ($\lesssim 2000$ yr) SNRs accelerate electrons in very thin regions around shock fronts.

4.2. Comments on Individual SNRs

4.2.1. Cas A

We analyzed filaments thinner than that by Vink & Laming (2003), and the former has harder spectra than the latter. This fact may imply that the magnetic field around our filaments is stronger than that around the filament by Vink & Laming (2003). Based on analysis of the filament-like structure in Cas A by Vink & Laming (2003), Berezhko & Völk (2004) estimated the magnetic field around the structure to be $\sim 500\ \mu$G, generated by the cosmic rays themselves (Lucek & Bell 2000). Our thinner filaments may have a larger magnetic field according to their discussion.

4.2.2. Kepler's Remnant

As for Kepler, since there is no report about nonthermal filaments, this is the first analysis of them. Cassam-Chenaï et al. (2004) reported that the southeastern edge of the SNR emits nonthermal X-rays with *XMM-Newton*. Their spectral parameters are consistent with ours. Therefore, the region by Cassam-Chenaï et al. (2004) may be a part of our filaments.

4.2.3. Tycho's Remnant

Our spectral results are roughly consistent with the results by Hwang et al. (2002), although the regions for spectral analysis are slightly different, except for the S abundance in the NEI model. The difference may come mainly from selection of the different background regions; we chose them not from out of the SNR, but from just at the downstream side of the filaments. We could thus extract pure nonthermal emission.

4.2.4. RCW 86

We reconfirmed the result of spectral analysis by Rho et al. (2002). A similar consideration of the magnetic field in the SN 1006 case as discussed by Yamazaki et al. (2004) may be possible, although the filaments are very clumpy and we may have to consider the curvature effect suggested by Berezhko et al. (2003). Together with the shock velocity of 562 km s^{-1} (Ghavamian et al. 2001) and results of spatial and spectral analyses (see previous sections), we estimated that the magnetic field around the filaments is ~ 4–12 μG (see also Bamba 2004). Watanabe et al. (2003) reported on TeV gamma-ray observations of the southwestern region of this remnant using the CANGAROO telescope. According to our results, inverse Compton TeV gamma rays may be detected with the current TeV gamma-ray telescopes. The estimated flux of inverse Compton emission is $\sim 6 \times 10^{-13}(B_d/10\ \mu\text{G})^{-2}$ ergs s^{-1} cm^{-2}.

4.3. Correlations between the Age and Spatial and Spectral Parameters

We found thin and nonthermal filaments in four historical SNRs, which may be acceleration sites of high-energy electrons. Their scale widths and spectral parameters include a lot of information about physical parameters inevitable for understanding acceleration on the shock, such as the gyroradius of electrons, the magnetic field configuration, and so on, as already suggested by Bamba et al. (2003b) in the SN 1006 case. Furthermore, a correlation between the age of SNRs and the spatial and spectral parameters might represent their time evolution in a single SNR, although we should consider the characteristics of the individual source. In this section we consider some correlation between the age and the physical parameters as a rough discussion about the time evolution.

Figure 4a represents the average scale width weighted by the flux of each filament (w_u and w_d in units of pc) as a function of the age (t_{age} in units of yr) for five historical SNRs; we analyzed four, and one was from the previous results of SN 1006 (Bamba et al. 2003b). The distances to the SNRs are fixed to previously estimated values (see § 3). The panel shows that in all SNRs, both w_u and w_d are quite smaller than the SNR radii. Moreover, there is a positive correlation between w_d and t_{age}; the scale width becomes larger as the SNR becomes older. We fitted them with a power-law function as a tentative model and obtain

$$w_d = 3.0^{+0.7}_{-0.6} \times 10^{-6} t_{\text{age}}^{1.60^{+0.01}_{-0.30}}, \qquad (2)$$

with the reduced χ^2 of 9.68/3. Hereafter the errors indicate 90% confidence regions. The index is larger than that for the shock width of thermal gas derived from the Sedov solution ($=\frac{2}{5}$), although we reached no definite conclusion because the fittings were rejected statistically.

Figures 4b and 4c show the plots of photon indices in the power-law fittings versus the age (t_{age}) and $\nu_{\text{roll-off}}$ (Hz) of the SRCUT model versus t_{age}, respectively. The spectrum seems to grow softer in the very young phase (less than 500 yr), whereas the spectral parameters remain constant at 1000–2000 years old. Since the error is too large, especially in the young phase, we gave up modeling the time evolution of the spectral parameters.

We searched for another parameter that has a clear correlation with time and found a tentative function,

$$\mathcal{B} = \nu_{\text{roll-off}} w_d^{-2}. \qquad (3)$$

Figure 4d represents the relation between t_{age} and $\mathcal{B}$. It shows monotonous decay, and a power-law fitting ($\mathcal{B} = C t_{\text{age}}^{\alpha}$) was accepted statistically with best-fit values of

$$C = 2.6^{+1.2}_{-1.4} \times 10^{27}, \qquad (4)$$

$$\alpha = -2.96^{+0.11}_{-0.06}, \qquad (5)$$

with a reduced χ^2 of 2.03/3, respectively. This result implies that the function $\mathcal{B}$ might include some physical quantities that evolve with time. We checked the uncertainty of $\mathcal{B}$ due to the change of s, as already discussed in § 4.1, and found that the best-fit value does not change although error regions become 10 times larger. Therefore, the uncertainty of s cannot change our results.

Here we create a scenario in order to explain the time evolution of $\mathcal{B}$. Our assumption is that the spatial profile found in our present
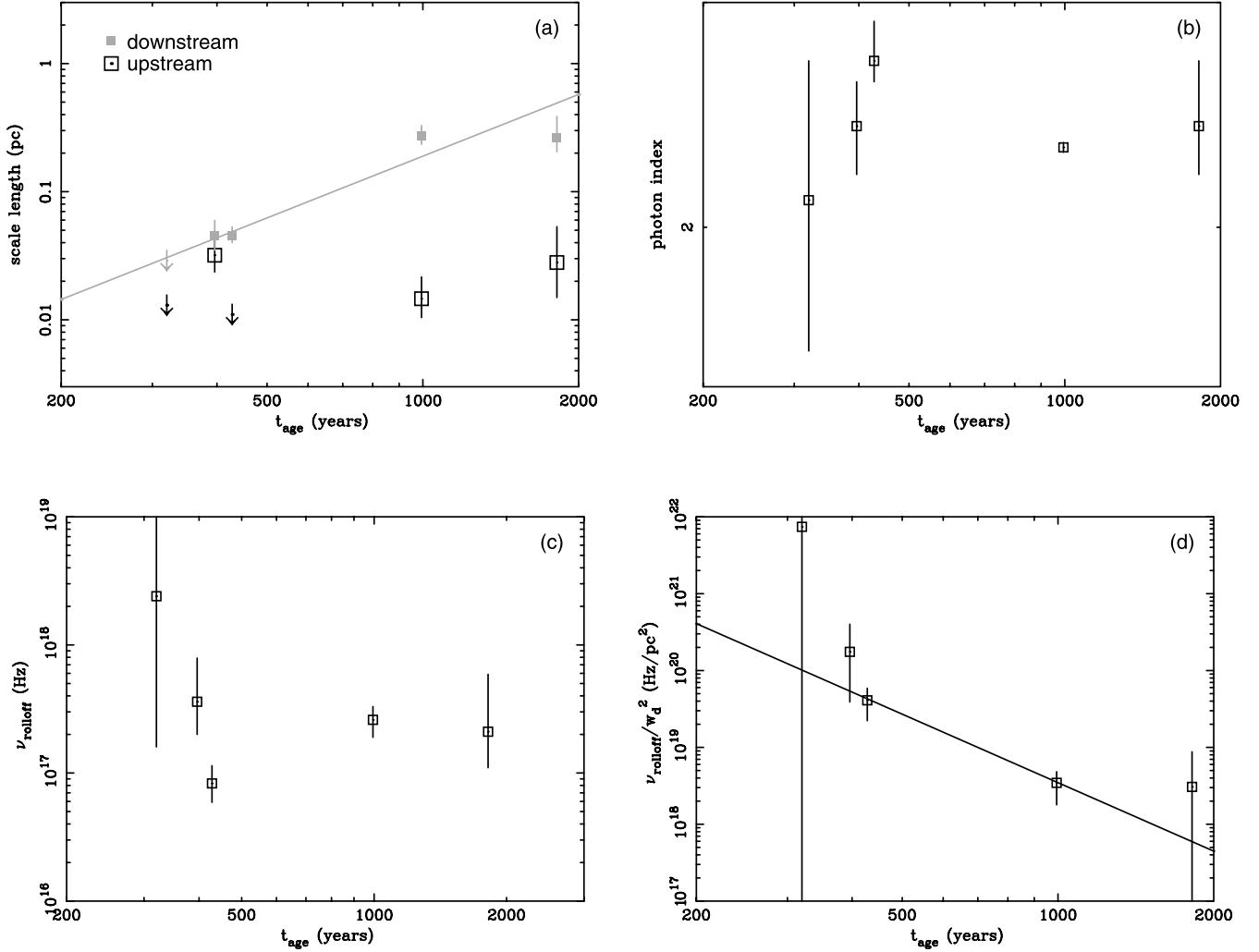
Fig. 4.—Time evolutions of parameters: (*a*) time vs. scale width; (*b*) photon index of power-law fitting; (*c*) $\nu_{\text{roll-off}}$ of SRCUT model fitting; and (*d*) $\mathcal{B} \equiv \nu_{\text{roll-off}}/w_d^2$. Solid lines represent best-fit models for each plot (see text).

analysis reflects that of accelerated electrons (Bamba et al. 2003b; Yamazaki et al. 2004). The maximum energy of accelerated electrons, $E_{\max}$, is determined by the age of the SNR, or the synchrotron energy loss, as $t_{\text{acc}} \sim \min\{t_{\text{age}}, t_{\text{loss}}\}$, where t_{acc} and t_{loss} are the acceleration and the synchrotron loss timescale, respectively (Yamazaki et al. 2004). Then we simply obtain the scale width of the accelerated electrons in the radial direction, Δ_d, as $\Delta_d \sim v_d \min\{t_{\text{age}}, t_{\text{loss}}\} \sim v_d t_{\text{acc}}$, where v_d is the downstream fluid velocity. The acceleration time t_{acc} is on the order of K/v_s^2, where v_s and K are the shock velocity and the diffusion coefficient, respectively. The quantity K is assumed to be proportional to the gyroradius of the accelerated electrons, $r_g = E_{\max}/eB_d$, where B_d is the downstream magnetic field (Drury 1983; Yamazaki et al. 2004). As a result, we find $\Delta_d \sim K/v_s \propto B_d^{-1} E_{\max} v_s^{-1}$. Because of the projection (curvature) effect, observed apparent scale width in the downstream region, w_d, differs from Δ_d (e.g., Berezhko & Völk 2004). The ratio w_d/Δ_d depends on uncertainty of the radial profile of the accelerated electron distribution downstream. It is found that for sufficiently small Δ_d compared with the local curvature radius, the ratio w_d/Δ_d is about 7, 5, or 1 when we assume the exponential, Gaussian, or top-hat form of the downstream radial profile, respectively. Hence, it may be assumed that the ratio w_d/Δ_d (~ 3) remains unchanged within a factor of 3, so we find $w_d \propto \Delta_d \propto B_d^{-1} E_{\max} v_s^{-1}$. The value of $\nu_{\text{roll-off}}$ is proportional to $B_d E_{\max}^2$ (Reynolds & Keohane 1999). Therefore, the quantity $\mathcal{B}$ is

proportional to $B_d^3 v_s^2$. The time evolution of $\mathcal{B}$ may represent that of $B_d^3 v_s^2$.

Let us consider the time evolution of the magnetic field and the shock velocity as $B_d \propto t_{\text{age}}^{-l}$ and $v_s \propto t_{\text{age}}^{-m}$, respectively. The index, m, changes from 0 to $\frac{3}{5}$ as SNRs evolve from the free-expansion phase to the Sedov phase. Together with the observational fact of equation (5), the index l takes the value of $0.57 - 1.02$. Our result suggests that the magnetic field decreases as the SNR ages. This is the first observational implication of the time evolution of the magnetic field in the SNR.

The most interesting case is $l = 0.6$, which is allowed when SNRs are in the Sedov phase ($m = 0.6$). In this case, since the density of the thermal plasma is almost constant, the energy density of the magnetic field ($u_B \propto B_d^2$) and the kinetic and thermal energy densities of the shock ($u_{\text{th}} \propto$ shock temperature and $u_{\text{kin}} \propto v_s^2$) evolve according to the same time dependency (index $= -1.2$). The time evolution of the energy density of accelerated protons (u_p) may also be discussed from the relations by Lucek & Bell (2000) as

$$u_p = \frac{v_s}{v_A} u_B \propto B_d v_s \propto t_{\text{age}}^{-1.2}, \qquad (6)$$

where $v_A \equiv B/(4\pi\rho)^{1/2}$ and ρ are the Alfvén velocity and the fluid density, respectively, suggesting that accelerated protons

in an SNR evolve with the same energy density evolutions as those of the other energy carriers. Since Bamba et al. (2003b) indicated that these energy densities are roughly in equipartition with each other, our result implies that they evolve while maintaining equipartition. Bell & Lucek (2001) suggested theoretically that the magnetic field on the shock evolves according to the same time dependency as the shock velocity, which is consistent with our result.

There remain many unsolved problems that we should consider. The value of w_d depends on many parameters that we have ignored, such as the curvature effect, the angle between the magnetic field and the shock normal, the degree of turbulence, and so on. Solving these problems is beyond the scope of our work and will be considered in Yamazaki et al. (2005).

5. SUMMARY

We have conducted systematic spectral and spatial analyses of filamentary structures in historical SNRs for the first time. A summary of our results is as follows:

1. We discovered very thin filaments on the outer edges of four historical SNRs: Cas A, Kepler, Tycho, and RCW 86. The scale widths were measured for the first time; they are below or the same as the PSF size of *Chandra* and 0.01–0.4 pc on the upstream and downstream sides of the emission peak, respectively.

2. Although both thermal and nonthermal spectral models can reproduce the spectra of the filaments, the former is unlikely since it requires an unrealistic high temperature and low abundances. The photon indices (~ 2–3) and $\nu_{\mathrm{roll\text{-}off}}$ ($\sim 10^{16}$–10^{18} Hz) of nonthermal models suggest that the synchrotron X-ray emission from electrons accelerated via DSA, in a similar way to the SN 1006 case.

3. The value of w_d (see eq. [2]) becomes larger as the SNR ages.

4. The spectra of filaments might become softer as the SNR ages in the phase of $t_{\mathrm{age}} \lesssim 500$ yr, whereas it does not change when 1000 yr $\lesssim t_{\mathrm{age}} \lesssim 2000$ yr, although there is no definite conclusion because of a lack of statistics.

5. The time evolution of a tentative function $\mathcal{B} = \nu_{\mathrm{roll\text{-}off}}/w_d^2$ was analyzed, and it has a clear negative correlation with t_{age} with the index of approximately -3. This may imply that the downstream magnetic field decreases with the index (l) of 0.6–1.0. When $l = 0.6$, energy densities of magnetic field, shock (thermal and kinetic), and cosmic rays evolve while keeping equipartition with each other.

REFERENCES

Allen, G. E., et al. 1997, ApJ, 487, L97
Anders, E., & Grevesse, N. 1989, Geochim. Cosmochim. Acta, 53, 197
Bamba, A. 2004, Ph.D. thesis, Kyoto Univ.
Bamba, A., Tomida, H., & Koyama, K. 2000, PASJ, 52, 1157
Bamba, A., Ueno, M., Koyama, K., & Yamauchi, S. 2001, PASJ, 53, L21
———. 2003a, ApJ, 589, 253
Bamba, A., Yamazaki, R., Ueno, M., & Koyama, K. 2003b, ApJ, 589, 827
Bell, A. R. 1978, MNRAS, 182, 443
Bell, A. R., & Lucek, S. G. 2001, MNRAS, 321, 433
Berezhko, E. G., Ksenofontov, L. T., & Völk, H. J. 2003, A&A, 412, L11
Berezhko, E. G., & Völk, H. J. 2004, A&A, 419, L27
Blandford, R. D., & Eichler, D. 1987, Phys. Rep., 154, 1
Blandford, R. D., & Ostriker, J. P. 1978, ApJ, 221, L29
Borkowski, K. J., Lyerly, W. J., & Reynolds, S. P. 2001a, ApJ, 548, 820
Borkowski, K. J., Rho, J., Reynolds, S. P., & Dyer, K. K. 2001b, ApJ, 550, 334
Cassam-Chenaï, G., Decourchelle, A., Ballet, J., Hwang, U., Hughes, J. P., & Petre, R. 2004, A&A, 414, 545
Caswell, J. L., Clark, D. H., & Crawford, D. F. 1975, Australian J. Phys. Astrophys. Suppl., 39
Chin, Y. N., & Huang, Y. L. 1994, Nature, 371, 398
Clark, D. H., & Stephenson, F. R. 1977, The Historical Supernovae (1st ed.; Oxford: Pergamon)
Decourchelle, A., et al. 2001, A&A, 365, L218
DeLaney, T., Koralesky, B., Rudnick, L., & Dickel, J. R. 2002, ApJ, 580, 914
Drury, L. O'C. 1983, Rep. Prog. Phys., 46, 973
Favata, F., et al. 1997, A&A, 324, L49
Fan You. 432, Houhanshu, 6. 3260 (reprint; Hong Kong: Chung-hua [1971])
Fink, H. H., Asaoka, I., Brinkmann, W., Kawai, N., & Koyama, K. 1994, A&A, 283, 635
Flamsteed, J. 1725, Historia Coelestis Britannicae (London: H. Meere)
Garmire, G., Feigelson, E. D., Broos, P., Hillenbrand, L. A., Pravdo, S. H., Townsley, L., & Tsuboi, Y. 2000, AJ, 120, 1426
Ghavamian, P., Raymond, J., Smith, R. C., & Hartigan, P. 2001, ApJ, 547, 995
Green, D. A. 2004, A Catalogue of Galactic Supernova Remnants (2004 January version; Cambridge: Mullard Radio Astronomy Obs.), http://www.mrao.cam.ac.uk/surveys/snrs
Hess, V. F. 1912, Phys. Zeits., 13, 1084
Hester, J. J. 1987, ApJ, 314, 187
Hwang, U., Decourchelle, A., Holt, S. S., & Petre, R. 2002, ApJ, 581, 1101
Jones, F. C., & Ellison, D. C. 1991, Space Sci. Rev., 58, 259

Kaastra, J. S., Asaoka, I., Koyama, K., & Yamauchi, S. 1992, A&A, 264, 654
Kamper, K. W., & van den Bergh, S. 1978, ApJ, 224, 851
Katz-Stone, D. M., Kassim, N. E., Lazio, T. J. W., & O'Donnell, R. 2000, ApJ, 529, 453
Kepler, J. 1606, De Stella Nova (Prague: P. Sessii)
Koyama, K., Kinugasa, K., Matsuzaki, K., Nishiuchi, M., Sugizaki, M., Torii, K., Yamauchi, S., & Aschenbach, B. 1997, PASJ, 49, L7
Koyama, K., Petre, R., Gotthelf, E. V., Hwang, U., Matsura, M., Ozaki, M., & Holt, S. S. 1995, Nature, 378, 255
Long, K. S., Reynolds, S. P., Raymond, J. C., Winkler, P. F., Dyer, K. K., & Petre, R. 2003, ApJ, 586, 1162
Lucek, S. G., & Bell, A. R. 2000, MNRAS, 314, 65
Malkov, E., & Drury, L. O'C. 2001, Rep. Prog. Phys., 64, 429
Morrison, R., & McCammon, D. 1983, ApJ, 270, 119
Petre, R., Allen, G. E., & Hwang, U. 1999, Astron. Nachr., 320, 199
Pravdo, S. H., & Smith, B. W. 1979, ApJ, 234, L195
Reed, J. E., Hester, J. J., Fabian, A. C., & Winkler, P. F. 1995, ApJ, 440, 706
Reynolds, S. P. 1998, ApJ, 493, 375
Reynolds, S. P., & Keohane, J. W. 1999, ApJ, 525, 368
Reynoso, E. M., & Goss, W. M. 1999, AJ, 118, 926
Rho, J., Dyer, K. K., Borkowski, K. J., & Reynolds, S. P. 2002, ApJ, 581, 1116
Rosado, M., Ambrocio-Cruz, P., Le Coarer, E., & Marcelin, M. 1996, A&A, 315, 243
Slane, P., Gaensler, B. M., Dame, T. M., Hughes, J. P., Plucinsky, P. P., & Green, A. 1999, ApJ, 525, 357
Slane, P., Hughes, J. P., Edgar, R. J., Plucinsky, P. P., Miyata, E., Tsunemi, H., & Aschenbach, B. 2001, ApJ, 548, 814
The, L.-S., Leising, M. D., Kurfess, J. D., Johnson, W. N., Hartmann, D. H., Gehrels, N., Grove, J. E., & Purcell, W. R. 1996, A&AS, 120, 357
Tycho, B. 1573, De Stella Nova (Copenhagen: Laurenentius)
Ueno, M., Bamba, A., Koyama, K., & Ebisawa, K. 2003, ApJ, 588, 338
Vink, J., & Laming, J. M. 2003, ApJ, 584, 758
Watanabe, S., et al. 2003, in Proc. 28th Int. Cosmic Ray Conf. (Tsukuba), 2397
Weisskopf, M. C., Brinkman, B., Canizares, C., Garmire, G., Murray, S., & Van Speybroeck, L. P. 2002, PASP, 114, 1
Winkler, P. F., Gupta, G., & Long, K. S. 2003, ApJ, 585, 324
Yamaguchi, H., Ueno, M., Bamba, A., & Koyama, K. 2005, PASJ, 56, 1059
Yamazaki, R., Bamba, A., Takahara, F., Yoshida, T., & Terasawa, T., 2005, ApJ, submitted
Yamazaki, R., Yoshida, T., Terasawa, T., Bamba, A., & Koyama, K. 2004, A&A, 416, 595